chemistry

MDPI

Article

The dielectric behaviour of protected HKUST-1

Simona Sorbara[1], Nicola Casati[2], Valentina Colombo[3,4], Filippo Bossola[4], and Piero Macchi[1]*

[1] Department of Chemistry, Materials and Chemical Engineering, Polytechnic of Milano, via Mancinelli 7, 20131, Milano (Italy)
[2] Laboratory for Synchrotron Radiation—Condensed Matter, Paul Scherrer Institute, Forschungstrasse 111, 5232 Villigen–PSI (Switzerland).
[3] Department of Chemistry, University of Milan, via Golgi 19, 20133, Milano (Italy).
[4] CNR - Institute of Chemical Sciences and Technologies (SCITEC) "Giulio Natta", via Golgi 19, 20133, Milano (Italy).

* Correspondence: piero.macchi@polimi.it Tel.: +390223993023

Abstract: We have investigated the adsorption properties and the dielectric behavior of a very well-known metal organic framework (MOF), namely $Cu_3(BTC)_2$ (known as HKUST-1; BTC=1,3,5-benzenetricarboxylate), before and after protection with some amines. This treatment has the purpose of reducing the inherent hygroscopic nature of HKUST-1, which is a serious drawback of its application of as low-dielectric constant (low-κ) material. Moreover, we have investigated the structure of HKUST-1 under a strong electric field, which confirms the robustness of the framework. Even under the dielectric perturbation, the water molecules adsorbed by the MOF remain almost invisible to X-ray diffraction apart from those directly bound to the metal ions. However, the replacement of H_2O with a more visible guest molecule like CH_2Br_2, makes the cavity that traps the guest more visible. Finally, with this work we demonstrate that impedance spectroscopy is a valuable tool to identify water sorption in porous materials, providing information, which is complementary to that of adsorption isotherms.

Keywords: metal organic frameworks, dielectric constant, adsorption properties

Citation: Sorbara, S.; Casati, N.; Colombo, V.; Bossola, F.; Macchi, P. The dielectric behavior of protected HKUST-1. *Chemistry* **2022**, *4*, xxx–xxx. https://doi.org/10.3390/xxxxx

Academic Editor: Firstname Lastname

Received: date
Accepted: date
Published: date

1. Introduction

Within the large array of applications of metal organic frameworks (MOFs), there is ever-growing attention for their use as materials for low dielectric constant (low-κ) devices, fundamental for the miniaturization of integrated circuits in informatics technology [1]. This is one of the main challenges in the current research on advanced and disruptive materials. Scientists and engineers try to design and fabricate new types of insulators alternative to the traditionally employed fiberglass, a composite of silica with a relatively high value of dielectric constant (κ= 3.9) [2], which is not adequate for further miniaturization of the devices. This deficiency causes, for example, a large cross-talk effect in microcircuits. For this reason, materials with lower κ are necessary to guarantee the expected advanced performances and to avoid unwanted processes.

The interest towards MOFs is motived by their very nature, i.e. very stable, tuneable, and highly porous solids that are often crystalline. Indeed, these are key-features for disruptive ultra-low-κ materials. In particular, the high porosity implies a very low content of matter (hence of electrons) in the volume overall spanned, which makes them ideal for achieving a perfect insulation and approaching the dielectric behaviour of vacuum itself (κ=1), which is of course the lowest limit. A material with at least ca. 50% of empty space inside should be able to guarantee $\kappa < 2$, which is one of the targets for new generation low-κ materials. Many MOFs are indeed known with such an empty volume inside their

structures and sufficient framework stability (i.e. rigidity) to preserve it over time and upon mechanical, thermal and chemical perturbation [3,4,5].

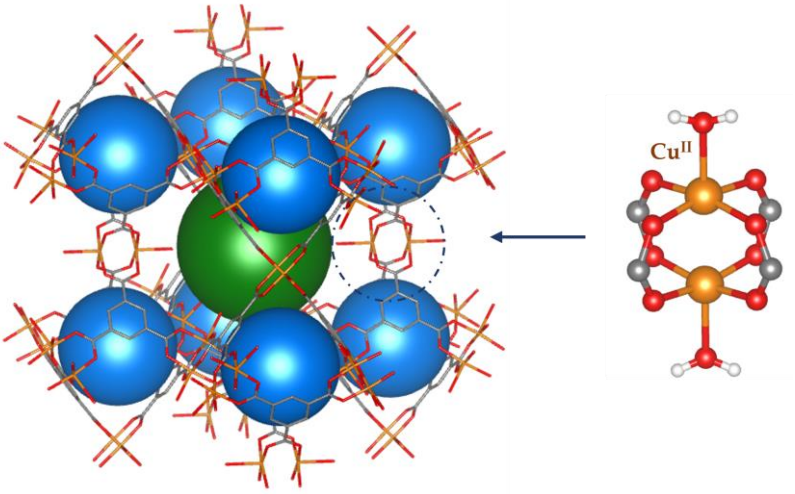

Figure 1. The structure of HKUST-1, an example of nano-porous MOFs. The secondary building unit (SBU) is represented on the right.

Although the above description addresses MOFs as seamlessly ideal low-κ materials, some pitfalls may affect their application. In fact, most MOFs are hygroscopic. This functionality is currently being exploited for water-sucking materials, designed to fight against drought [6]. However, for applications in micro- and nano-electronics, hygroscopicity is a fundamental defect, because it implies (partial) occupation of the pores with very mobile and highly polarizable water molecules, affecting the extraordinary dielectric behavior highlighted above.

Some possible strategies in the MOF design could tackle this problem. The objective is designing a hydrophobic material with the minimal loss of dielectric performance. This could be achieved using directly hydrophobic building blocks or otherwise by post-synthetic modifications of the MOF with the insertion of functional groups that can guarantee the requested hydrophobicity. These strategies, though, do not always lead to the desired material, because a perfect hydrophobicity may not be obtained by simply introducing some hydrophobic functional groups in the building blocks (normally in the organic linkers). In fact, the metals may remain sources of attraction for water molecules, unless completely saturated by the coordinated linkers. Moreover, the linkers may be ambivalent, featuring both hydrophobic and hydrophilic sites.

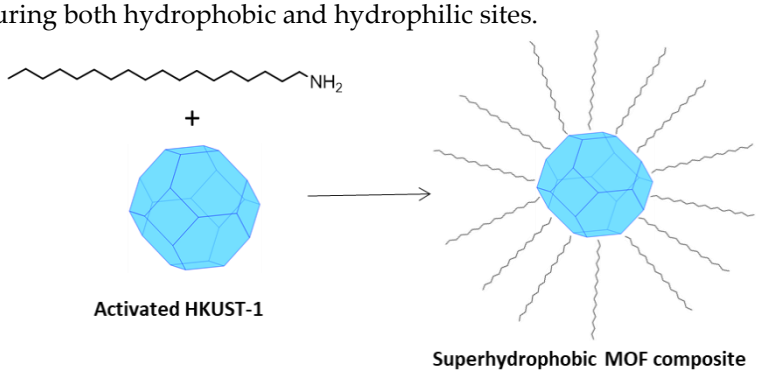

Figure 2. A schematic picture of the fabrication of super-hydrophobic MOF composite by means of long-chain alkyl amines (like OA). This picture is similar to Figure 1 of reference [8].

An alternative is protecting the pores of the MOFs to hamper the insertion of water molecules into the framework. This drastically reduces the MOF capacity to suck water

molecules, without affecting the internal structure or anyway with the minimal perturbation limited to the surface and few inner layers. One example is the coating approach with polydimethylsiloxane proposed by Zhang *et al.* [7].

Recently, Gao *et al.* [8] proposed a strategy to fabricate super-hydrophobic and super-oleophilic MOF composites, obtained from the surface reaction of the activated MOF (i.e. evacuated from content in the pores) with octadecyl-ammine (OA). The long alkyl chain of OA with low surface energy was grafted onto the surface of some highly porous MOFs, making them water-resistant and endowing the composites with admirable superhydrophobicity. The possible drawbacks for their application as low-κ material is the polarizability enhancement of the system due to the insertion of the amine itself, and the long-term stability especially in highly humid environment.

In this study, we focused on one of the most studied MOFs, namely $Cu_3(BTC)_2$ (see Figure 1), also known as HKUST-1 [9], where BTC stands for the deprotonated form of benzene-1,3,5-tricarboxylic acid (noteworthy, sometime the linker is reported in the literature as trimesic acid anion, TMA). As well-known, HKUST-1 features a large porosity, up to ca. 70% (as calculated with a probe radius of 1.2 Å), a very high chemical and thermal stability, but it is very hygroscopic. Its hydrophilicity is in the first instance related to the unsaturated square planar Cu(II) ions, present in HKUST-1 in the form of classical copper acetate paddle-wheel geometry (see Figure 1). Noteworthy, this coordination occurs along a Jahn-Teller distortion direction and is not the strongest binding to the metal ion. Nevertheless the apical vacancy at the Cu(II) ion represents a preferential adsorption site for water molecules, found already in the as-synthetized material. This however explains only a small portion of the overall hydrophilicity that increases through more traditional electrostatic interactions between water molecules and other sites of the linkers.

For these reasons, HKUST-1 represents an ideal candidate to test if the protection methods described above could be efficient and adopted to make highly porous, but hygroscopic MOFs, suitable low-κ materials. In addition, we have tested HKUST-1 under the perturbation of an electric field, because its stability in these conditions has not been ascertained so far. Indeed, until now, only theoretical calculations have been reported on some MOFs' crystal structure under electric field, but experiments have not been reported. For example, Ghoufi *et al.* [10] have studied a flexible MOF, MIL-53, that, unfortunately, cannot be obtained in single crystal form.

The experiments on dielectric constant and water adsorption that we report here are supported by theoretical calculations of the polarizabilities of the species (building blocks of HKUST-1 and amines used for the protection) in order to gain insight into the electronic structure of the material under the perturbation of an electric field and provide useful parameters for efficient design of new materials based on this approach.

2. Materials and Methods

2.1. Synthesis.

The hydrated form of $Cu_3(BTC)_2$ (HKUST-1) was prepared according to the reported method [*11*]. Microcrystalline pellets of HKUST-1 were activated by heating to 200 °C for 20 h at 10^{-2} mbar. As reported previously by Schlichte *et al.* [*12*], this treatment is sufficient for a complete removal of all guest molecules.

For a better visualization of the guest molecules inside HKUST-1, water was exchanged with CH_2Br_2. For this purpose, a HKUST-1 sample was activated in vacuum at high temperature and 100 mg were plunged in 5 mL of CH_2Br_2.

Table 1. The amines used for protection of HKUST-1.

RNH_2	Acronym	Amount of RNH_2 (g)	Amount of HKUST-1 (g)	Composite Color
Octadecylamine	OA	1.348	1.000	Dark Blue
Decylamine	DA	0.786	1.000	Dark Blue
Amylamine	AM	0.435	1.000	Dark Blue
1-Naphthylamine	1NTA	0.716	1.000	Black
Aniline	AN	0.465	1.000	Dark Green
3-Phenyl-1-propylamine	3P1PA	0.676	1.000	Dark Blue

2.2. MOF surface protection.

The surface reactions of the activated HKUST-1 with different amines were carried out following the prescription by Gao *et al.* [8] for octadecyl amine. A solution of toluene with the activated MOF and the amine (with a concentration of 10 mM) was stirred at 120 °C for 24 h under nitrogen. In Table 1, we report the quantities adopted for each reaction and the corresponding color observed for the powder of the composite material.

2.3. Dielectric constant measurement.

The dielectric constant is determined through impedance spectroscopy. The measurements were carried out with a Solartron impedance/Gain-Phase analyzer ModulabXM equipped with XM MFRA 1 MHz and XM MAT 1 MHz control modules. A 12962A sample holder was used with dried powder pellet samples with a diameter of 13 mm prepared by applying a force of ca. 15 kN (corresponding to a pressure of ca. 0.1 GPa). The sample holder consists of a two brass parallel electrodes capacitor, provided with a guard ring, which reduces the fringing effect of stray fields at the edge of tested materials. The measurement parameters were controlled with the ModulabXM software. The measurement setup consists of a fixed mode generator voltage level of 0 V with amplitude of 100 mV and a frequency sweep from 1 Hz to 1 MHz. The electronic field is applied between the two electrodes, across a measured thickness of the sample, at room temperature.

All the pellets activated at 200 °C for 20 h at 10^{-2} mbar were loaded into the sample holder in a glovebox under N_2 atmosphere. After the initial measurements at time t_0, all the pellets were expose to a stable air humidity of ca. 60% and the dielectric constant was measured at variable intervals: with a frequency of 10 minutes for the first half-hour, then gradually less frequent up to t_∞ = 13 days after activation. For each sample, we performed at least two measurements and the reported results are the averaged values.

2.4. X-ray diffraction

Synchrotron X-ray diffraction data were collected at the Material Science beamline of the Swiss Light Source (Paul Scherrer Institute, Switzerland) [13]. The system used to collect diffraction data under the electric field consists of two stainless steel electrodes of 0.4 mm diameter and a length of 3.5 mm. A single crystal sample was mounted with silver paste on one of the two electrodes, while the other was placed at ~1 mm distance. The axial system was mounted vertically and the electric field resulted applied along this direction, perpendicular to the incoming (horizontal) beam. The highest applicable voltage is limited to 2kV due to sparks generated during the diffraction experiments by the ionizing x-rays. For sake of safety, a potential of 1,5 kV was applied. Because the typical dimension of the specimen is ~ 100 μm of linear dimensions, the applied electric field resulted of the order of magnitude of 0,01 GV/m.

For HKUST-1 (compound **1**), the diffraction was collected on the very same sample before, during and after the application of electric field with radiation doses of ca. 25

minutes separated by 5 minutes (for the data collection after removing the electric field a double dose was planned, but only the first run was eventually used for the refinements, due to the observed sample decay). For HKUST-1@CH_2Br_2 (compound **2**), the data collection before applying the field was carried out on a different sample in order to reduce the possible sample decay, whereas a second sample was collected during and after the application of the field (for 50 minute and 15 minutes, respectively, after 15 minutes of relaxation).

A monochromatic beam of a radiation with energy ~25.2 keV was adopted, each time calibrated by the diffraction of a Si standard. The 2D diffraction images were recorded with the Dectris-Pilatus 6M 2D detector and integrated using Rigaku-Oxford Diffraction Crysalis [14]. Crystal structure refinements were carried out with Olex2 [15], starting from a known model of unperturbed HKUST-1 [27]. The software Mercury [16] was used to draw the crystal structures and calculate the void volume.

Powder X-ray diffraction was performed on synthesized samples, before and after the protection with amines. The data were collected with a Bruker D2 phaser diffractometer, working with 30 kV and 10 mA, using CuKα monochromatized radiation.

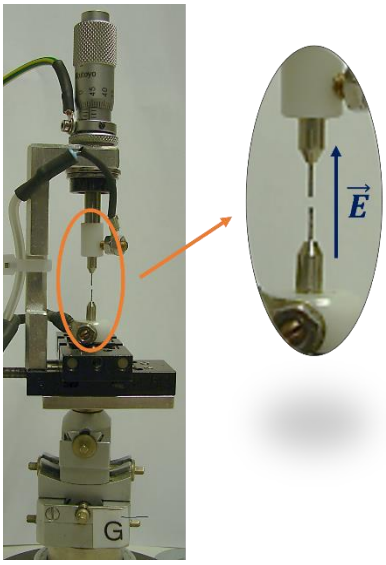

Figure 3. The set-up for the measurements under electric field at the Swiss-Light Source of Paul-Scherrer Institute.

2.5. Water absorption isotherms

Water adsorption isotherms were measured with a Micromeritics ASAP2020 at 295 K on samples previously degassed for 12 h at 180 °C in high vacuum. The water physisorption properties of three powder samples were evaluated: HKUST-1, to have a blank; 3P1PA and DA, which seem to have the best performances between aromatic and alkyl amine, respectively. In addition, to confirm the different adsorption capacity of a pellet in comparison to a powder, water adsorption isotherm of a pellet of DA was also performed.

2.6. Theoretical calculations.

Density functional theory (DFT) calculations on all the protecting ammines and their interactions with the HKUST-1 frameworks were performed employing the B3LYP functional [17,18] in combination with the def2TZVP basis set [19,20] using the software Gaussian16 [21] on the hpc-supercomputer Galileo-100 of the Italian CINECA. The amines geometries were optimized and their polarizabilitiy was calculated applying couple-perturbed Kohn-Sham theory. The atomic polarizability tensors were calculated via numerical differentiations of the total atomic dipoles, using the software PolaBer [22]. An electric field of 0.0001 atomic units was applied in positive and negative x, y and z directions and

the corresponding electron densities have been analyzed with the quantum theory of atoms in molecules (QTAIM) [23] using AimAll [24] that calculates atomic dipole moments, following the scheme proposed by Bader and Keith [25] and modified by Krawczuk *et al.* [22]. The inherent asymmetry of the atomic polarizabilities is overcome by the symmetrization scheme of Nye [26].

3. Results and discussion

3.1. HKUST-1 under electric field

HKUST-1 crystallizes in the cubic space group $Fm\bar{3}m$ featuring a high fraction of unoccupied volume, at least ideally, i.e. assuming that all the pores are empty and that all metal ions are not coordinated along the apical site. The three-dimensional periodic structure is generated by the binuclear Cu(II) paddlewheel secondary building units (SBUs) connected via the tritopic BTC organic linker (see Figure 1). Two kinds of intersecting pores are present with diameters of ca. 10 and 15 Å (see Figure 1). The large (octahedral) cavity in the centre of the unit cell (represented in green in Figure 1) is crystallographically equivalent to cavities in the middle of unit cell edges (not shown in the picture), and topologically identical to those at the centre of the faces and at the vertexes of the cell (not show in Figure 1 for sake of simplicity; for more details see the Figure S1 in the Supporting Information). These two cavities correspond to the sites occupied by Na and Cl in NaCl. The smaller (blue) cavity, instead, sits on a tetrahedral site. Noteworthy the large cavities are directly interconnected through channels along the main crystallographic directions so that they give rise to uninterrupted empty volumes, whereas the smaller cavities are more closed and connected only to the large cavities through smaller apertures.

After activation, if exposed to a humid atmosphere HKUST-1 rapidly adsorbs water molecules, a phenomenon which is easily appreciated from the change of colour from dark blue to cyan. Water molecules can easily access both kinds of pores and even anchor to the internal surfaces of the MOF. According to a previous study, see Scatena *et al.* [27], we can identify three kinds of water molecules: (a) those freely moving in the pores without any strong interaction with the framework; (b) those connected through hydrogen bond to the framework linkers; (c) those weakly coordinated to the metal nodes of the framework along the Jahn-Teller distorted direction (typical for Cu(II) ions). With X-ray diffraction on single crystals, only type (c) water molecules are (partially) visible because quite rigidly constrained to the metals and because of the Cu-Cu bond length increase, while all other H_2O molecules are not directly visible, and their presence can only be inferred through the analysis of the residual electron density inside the channels. Being a rigid, second generation [28] type of MOF, the volume increase due to hydration is very small.

Because of the high hydrophilicity, only under special conditions (namely after activation and in an anhydrous atmosphere), can HKUST-1 display the exceptionally low dielectric constant (κ~1.7, see [27]) predicted theoretically and guaranteed by the large voids of the structure, which is the main hypothesis suggesting MOFs as potentially good low-κ materials.

In the next paragraphs we discuss the methods to protect the $\{Cu_3(BTC)_2\}$ framework and obtain the same good dielectric behaviour even when an anhydrous atmosphere cannot be guaranteed. There are anyway other features required to elect a MOF like HKUST-1 as a good low-κ material. For example, HKUST-1 is known for its high thermal and chemical stability, as well as easy synthesis and tendency to form sufficiently large single crystals of good quality (hence ensuring a good reproducibility of the materials structural properties). One additional feature to check is the stability under electric field, which implies both the breakdown voltage (i.e., the field necessary to break the insulating behaviour) and the structural changes under the field (before the breakdown). Although some studies have reported the incipient conductance of HKUST-1 doped with guest molecules

like tetracyanoquinodimethane [29], to the best of our knowledge the breakdown voltage of pure $\{Cu_3(BTC)_2\}$ has not been established so far. Our interest anyway was for the structural stability under electric field. This study has two purposes: one is to assess the stability of the rigid framework structure under an applied electric field; the other is testing if water molecules inside the MOF channels can be somewhat visible through X-ray diffraction under electric field (that would order the guests). Water is indeed very mobile because it has a small mass and a large dipole, therefore easily oriented in an externally applied field. As anticipated above, the disorder of water molecules inside the framework channels of HKUST-1 is a drawback, because they do not contribute to Bragg diffraction peaks in a measurable way. On the other hand, a reordering of water molecules inside the channels may display clearer features in the diffraction pattern. However, because water does not contain heavy atoms, its contribution to x-ray diffraction remains small.

The adopted experimental procedures were designed in the following steps. Diffraction data were collected, at ambient temperature, with the electric field initially *off* taken as a benchmark of the unperturbed sample (experiment **1a**), then *on* (experiment **1b**) and eventually *off* again (experiment **1c**) to check effects after the application of a field (see experimental section for more details). To monitor the electric field effects, the structural models were refined using the framework atoms only (and including the oxygen atom of the water molecule directly coordinated to Cu), so that the corresponding F_o-F_c maps address the unassigned electron densities associated with solvent guests inside the pores, apart from experimental errors.

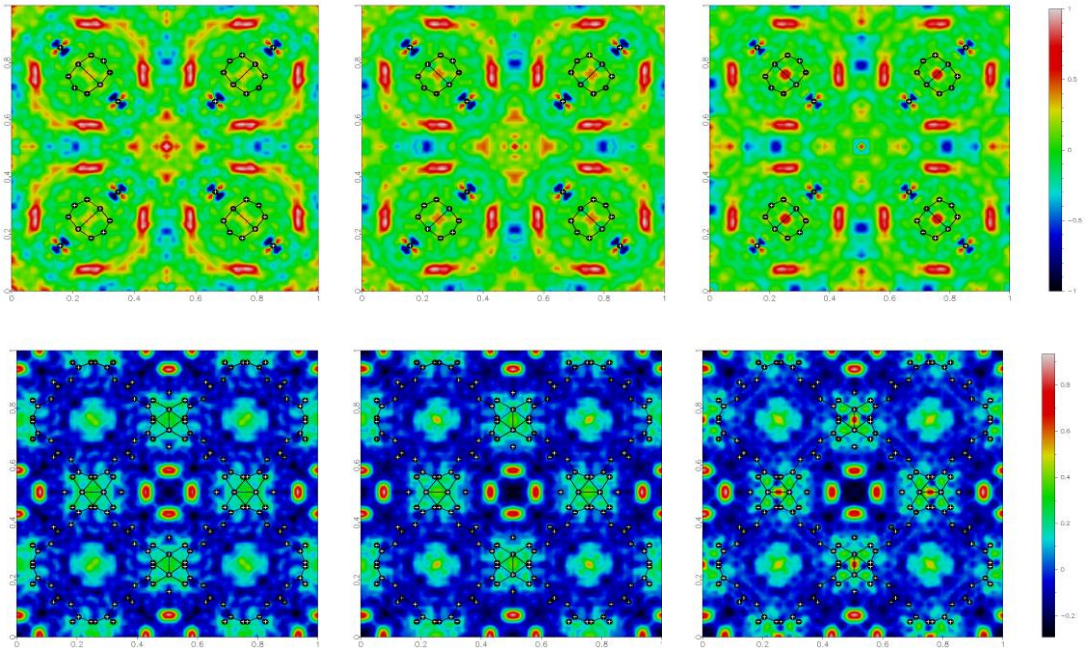

Figure 4: Residual electron density maps (obtained as Fourier summation of F_o-F_c) for HKUST-1 in the plane (x,y,0.5) on the top and (x,y,0.25) on the bottom, under different conditions: before, during and after the application of 1.5 kV potential generating an electric field at the sample of ca. 1.5×10^{-2} GV/m. The residual electron density values are colour coded, as shown on the right side.

The electron density maps (Figure 4) show slightly different sizes and shapes of the residuals depending on the applied field, indicating that the external stimulus produces some, albeit very small, effects to the guest water molecules inside the cavities. For example, a small decrease of the residual electron density inside the octahedral cavities is observed when applying the 1.5 kV voltage: the largest residual occurs at the octahedral cavity at the centre of the cell evolving from 1.4 to 1.0 $eÅ^{-3}$. Moreover, there seems to be some hysteresis because those effects persisted even after switching off the electric field.

No significant structural change was observed in the $\{Cu_3(BTC)_2\}$ framework, which confirms the stability of HKUST-1 in a relatively strong electric field, at least well above the realistic operation limits. In fact, the unit cell volume change is below 0,1%, within the typical variance observed in different experiments on the same sample. Moreover, all bond-distances and angles within the framework differ for less than 1σ.

In order to make the guest molecules more visible and test how they occupy the pores of the MOF, water was exchanged with another polar solvent containing heavier atoms, namely dibromomethane (see details in the experimental section). HKUST-1 maintained its crystallinity, which allowed to refine the structure (isostructural to the hydrated form of HKUST-1), through single-crystal X-ray diffraction. The experiment revealed quite well the CH_2Br_2 molecules, that seamlessly fit the tetrahedral cavities and partially occupy them, though of course in a disorder manner (the molecule belonging to a symmetry subgroup of T_d). Their occupancy remains stable over time, despite the well ascertained affinity of HKUST-1 for water. In the larger octahedral cavities, instead, there is little evidence of what is the content. The residuals at the centre of these cavities are larger than for the hydrated samples, which could be due either to a better phasing of the reflections thanks to the Br atoms, and/or to some CH_2Br_2 molecule being disordered along the channels (but not trapped as for the tetrahedral cavity). The CH_2Br_2 stability inside the MOF was evaluated not only by X-ray diffraction but also through bromine X-ray fluorescence, which does not decrease over the time, at least judging from the background intensity (mainly due to the fluorescence, considering that the detector was set to measure at an energy threshold below the K-edge of bromine).

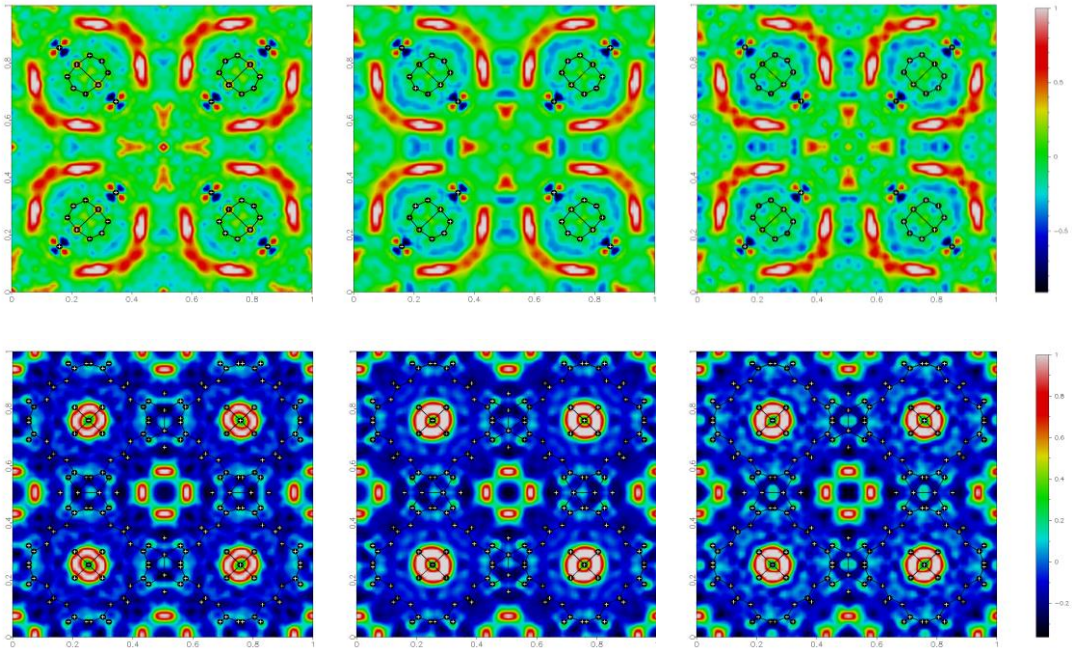

Figure 5: Residual electron density maps (obtained as Fourier summation of F_o-F_c) for HKUST-1@CH_2Br_2 in the plane (x,y,0.5) on the top and (x,y,0.25) on the bottom, under different conditions: before, during and after the application of 1.5 kV potential generating an electric field at the sample of ca. 1.5×10^{-2} GV/m. The electron density values are colour coded, as shown on the right side.

We also tested these samples under electric field. Because from the previous experiments on hydrated samples, we noticed that HKUST-1 suffers from radiation damage, the radiation dose was reduced (taking also advantage of the larger scattering power of Br). Moreover, the diffraction experiments were carried out on two different single crystals: one used for the experiment **2a** (without the field) and the other one for experiments **2b - 2c** (during and after the application of the field). Like for the hydrated forms, we calcu-

lated the Fourier difference maps (see Figure 5), including in the model the CH_2Br_2 molecules inside the tetrahedral cavities, whereas water molecules were not included in the refinement (apart from the oxygen atom of the water molecule coordinated to Cu).

Again, the application of the electric field only showed minor changes. First of all, no phase transition toward a polar space group was observed caused for example by the reordering of the CH_2Br_2 molecules. There is only a slight decrease of the (isotropic) atomic displacement parameter of Br (though strongly correlating with the occupancy). There is an increase of electron density in correspondence of CH_2Br_2 molecules, also visible in the maps of Figure 5. These effects are partly maintained even after switching off the field.

3.2. Dielectric behaviour of protected HKUST-1

Adopting the strategy proposed by Gao *et al.* [8] (see also the introduction), we have protected HKUST-1 with various amines, as described in the experimental section (see also Table 1). After the reaction, the crystallinity of the materials was tested with X-ray powder diffraction (see supporting information).

In order to test both the efficiency in enhancing the hydrophobic character of the MOF and preserving the same low-κ feature of the activated HKUST-1, we measured the impedance spectroscopy for all the samples and determined the dielectric constant. κ is not typically adopted as an indicator of hydrophobicity. For this reason, we have coupled the measurements with gravimetric analysis in order to estimate the amount of water adsorbed within specific time ranges. In the next paragraph, we also compare this technique with the more traditional water adsorption isotherms.

Table 2. Isotropic polarizabilities α_{ISO} of the amines used for the protection of HKUST-1 and their contribution to the high frequency dielectric constant of the material, assuming a full saturation of the Cu(II) sites (Theor. Δκ is the expected increase with respect to the ideally empty $Cu_3(BTC)_2$). For sake of reference, the experimental Δκ of the amine-protected HKUST-1 at 1MHz is reported (the reference being the unprotected HKUST-1). The discrepancy between the expected Δκ and the actually measured indicates the degree of saturation of the Cu(II) sites.

Protecting amine	α_{ISO} (Bohr^3)	Theor. Δκ	Expt. Δκ(1MHz)
Octadecylamine	234.7	1.15	0.11
Decylamine	133.9	0.65	0.18
Amylamine	71.7	0.35	0.32
1-Naphthylamine	125.6	0.61	0.39
Aniline	75.9	0.37	0.24
3-Phenyl-1-propylamine	112.8	0.55	0.27

For the dielectric constant measurements, two parameters are analysed: a) κ at high frequency (1 MHz, the highest value reachable by our instrumentation); b) κ at low frequency (1 Hz). At high frequency, the dielectric constant simply depends on the polarizable electron density of the material because the nuclear motion contribution is not activated yet. Therefore, the increase of κ (1 MHz) with respect to the as-activated material is directly proportional to the amount of matter (water) adsorbed per unit of volume. At low frequency, instead, the nature of the binding of water molecules to the MOF may result in higher or lower dielectric constant. In fact, as for example reported by Scatena *et al.* [27], water molecules coordinated to Cu(II) ions do not contribute to enhance κ at 1 Hz or lower, because they are quite tightly bound to the framework. Instead, molecules less tightly bound or free to move into the channel produce significant alteration of κ at 1 Hz, while only minimal at 1MHz. One could also consider the dielectric constant at lower frequencies, but the measurement would be significantly longer (the time being obviously inversely proportional to the frequency), without producing more information. Instead, a scan between 1MHz and 1 Hz (typically repeated in 10 cycles) takes only few seconds and

allows a series of measurements at regular time intervals after the exposition of the material to a humid atmosphere. This enables deriving precise adsorption kinetics curves.

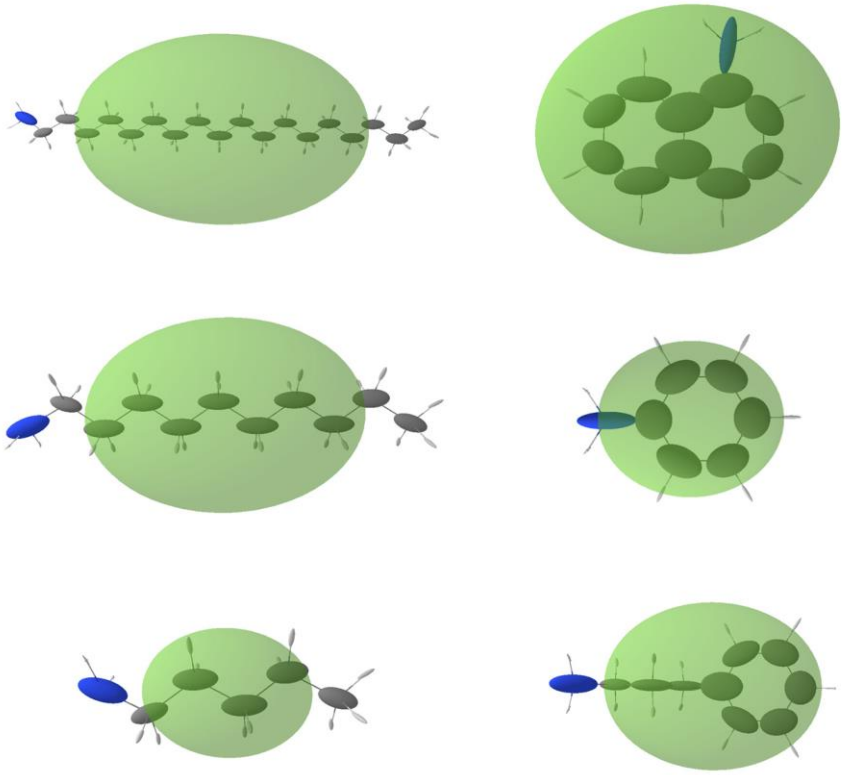

Figure 6: Molecular and distributed atomic polarizabilities calculated for all amines used in this work, using the software PolaBer [22]. Atomic polarizabilities are represented as atom-centered ellipsoids (coloured according to the atom type, white for H, grey for C and blue for N), scaled with 0.2 $Å^{-2}$ for proper representation in the plot. Molecular polarizabilities are in transparent green, centered at the center of mass of the molecule and multiplied for a scale factor of 0.1 $Å^{-2}$.

In Figure 7, we report the correlation between the density of adsorbed water (ρH_2O, based on gravimetry) and the two dielectric constant measurements [κ(1MHz) and κ(1 Hz)] for unprotected HKUST-1 (top plot) and all types of amine protected HKUST-1 that we prepared. As anticipated, the correlation between ρH_2O and κ(1MHz) is linear. Unprotected HKUST-1 after the activation features the lowest κ(1MHz) (1.78), whereas all the amine-protected materials have higher baselines that obviously depend on the surface reactant itself (see below). The slope of κ(1MHz) against ρH_2O is much larger for unprotected HKUST-1, compared to all amines (only the 1naphtil-amine HKUST-1, 1NTA, has a similar trend). This means that the adsorbed water molecules may occupy different sites in unprotected or protected HKUST-1, therefore being polarizable in different ways. This is seamlessly confirmed by the low frequency dielectric constant, which grows exponentially in unprotected HKUST-1 (and similarly in 1NTA protected), whereas it remains almost linear for all other amine-protected materials. The ideal saturation of all Cu(II) sites occurs for an adsorption of 0.078 g/cm^3 of H_2O.

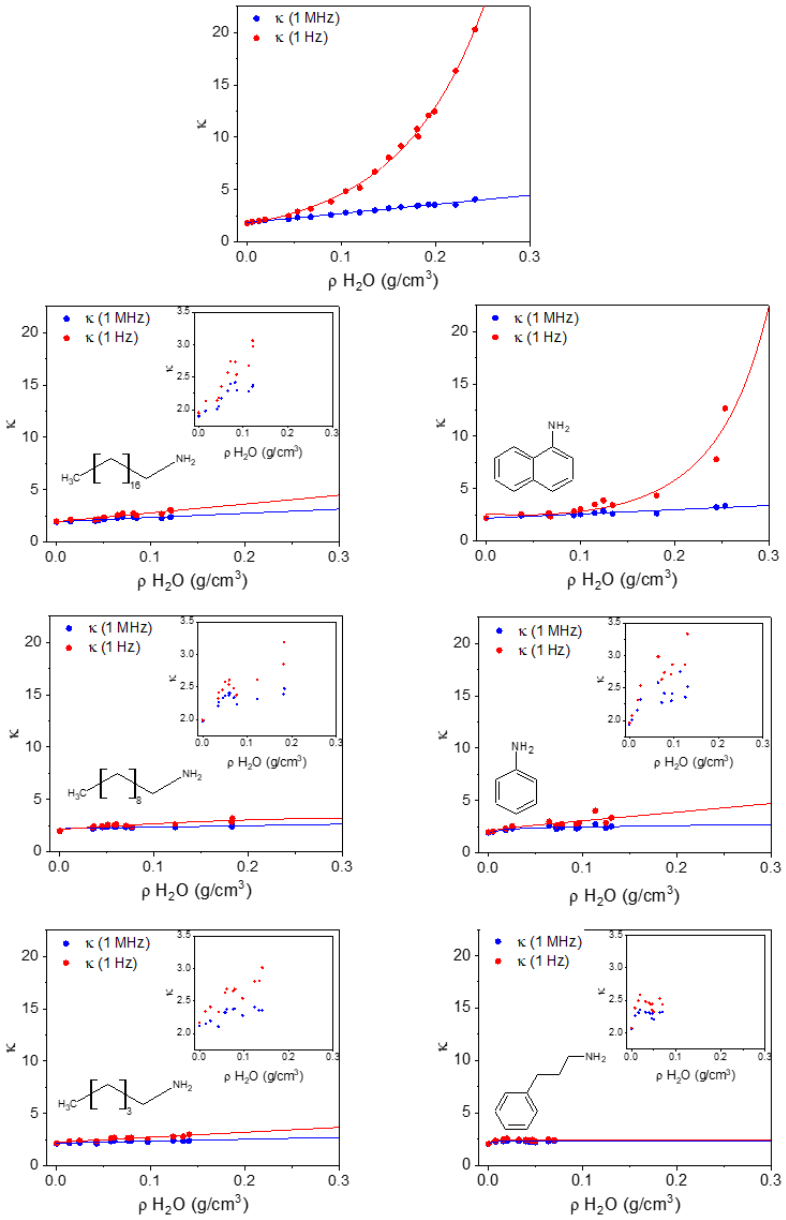

Figure 7: The dielectric constant at 1MHz (blue) and 1Hz (red) as a function of the mass density of adsorbed water in HKUST-1 and in all amine-protected species (left column alkyl amines; right column aromatic amines).

Because the full occupancy of these sites does not occur before other water molecules start occupying the cavities, the deviation of low-frequency κ from linearity (and from high frequency κ) begins for $\rho H_2O < 0.078$ g/cm³ in unprotected HKUST-1.

In 3P1PA protected HKUST-1 there is almost no difference between low and high frequency, as it occurs for activated HKUST-1 when measured in a protected atmosphere and therefore prevented from adsorbing water [27]. Nonetheless, the gravimetric analysis shows some water adsorption in 3P1PA, but the protection annihilates all negative effects of water sorption. The price to pay is a slightly larger κ compared with activated HKUST-1. For all other amine-protection, apart from 1NTA, the low frequency κ is anyway quite close to the high frequency, even though the saturation limit of Cu(II) sites is overcome and therefore water molecules surely bind other sites or are even free in the cavities of HKUST-1. Again, it seems that the effect of amine protection is that of severely reducing

the mobility of water molecules inside the channels, even though the surface reactants were not able to prevent water sorption.

In Table 2, the calculated polarizabilities of the amines are reported together with their expected contribution to the dielectric constant enhancement. Δκ are calculated assuming that the amines coordinate all the Cu(II) metal ions in the structure. This is obviously unlikely to occur and therefore the experimentally measured increases of dielectric constant with respect to unprotected HKUST-1 are smaller. Noteworthy, octadecylamine, the most hindered one, seems to occupy only 10% of the sites available, likely only those closer to the external surfaces of the crystallites. The smaller amylamine, instead, almost saturates them, given that the observed Δκ(1MHz) is close to the expected one. For the aromatic amines, the dielectric constant increase is 50-65% of the theoretical amount.

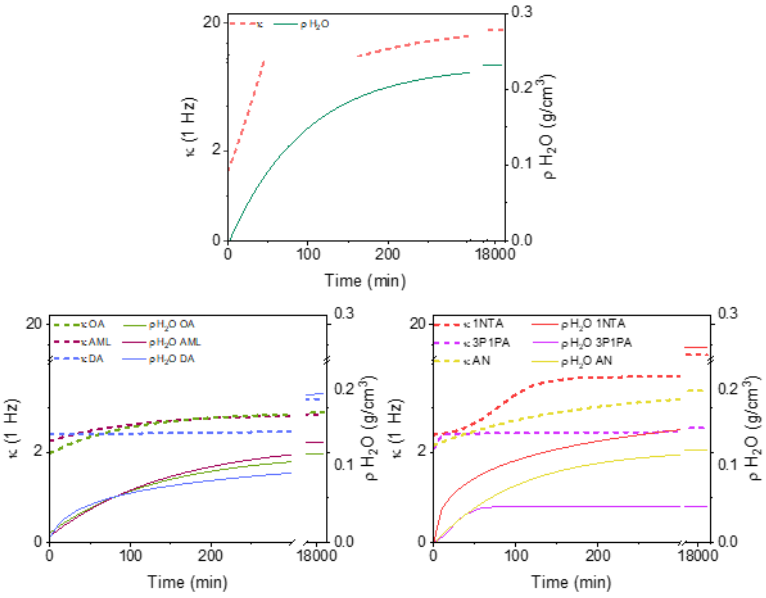

Figure 8: The dielectric constant at 1Hz and the mass density of adsorbed water as a function of time. Tope HKUST-1, bottom left alkyl amines, bottom right aromatic amines.

3.3. Correlation between isotherm adsorption curves and dielectric constant

The results presented in the previous paragraph concern the dielectric behaviour of protected HKUST-1 and clearly indicate that the surface reaction of amines significantly reduces the dielectric constant compared to unprotected HKUST-1, especially in the low frequency regime which is more sensitive to the mobility of polar guests.

The amount of water adsorbed (estimated from the weight increase of the measured pellets), can be verified with water adsorption isotherms. While adsorption isotherms of N_2 are used to measure the accessible surface area and pore volume, water adsorption measurements provide additional information due to the high polarity of the molecule and its hydrogen bond affinity, resulting in strong or weak interactions with the tested material. As reported by Canivet et *al.* [30], contradicting results on water adsorption isotherm are sometimes reported in the literature. HKUST-1 was found to be stable in water vapour by Alverez *et al.* [31], who reported a decreased capacity of adsorbing water, but no worsening for other gases. Other authors, instead, reported both a significant decrease of specific surface area and water capacity after water adsorption. [32,33].

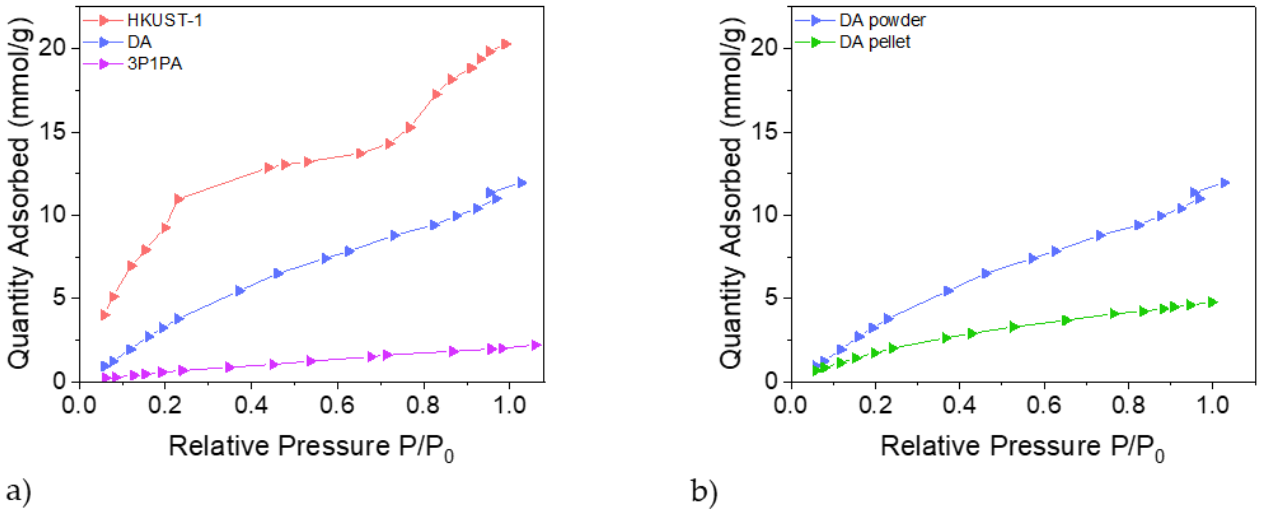

Figure 9. a) Quantity of water adsorbed per gram of unprotected HKUST-1, DA-protected and 3P1PA-protected substance as a function of the relative pressure; b) Quantity of water adsorbed per gram of DA-protected HKUST-1 as function of relative pressure for a powder and a pressed pellet. Due to the smaller exposed surface area, water adsorption for pellets is significantly lower.

From Figure 9, HKUST-1 shows a two steps adsorption process in the lower pressure, indicating two energetically different mechanisms, which is in accord with the literature [32]. First, water molecules bind the free copper sites. The second step in the adsorption isotherm indicates the filling of the large and small pores, which are less hydrophilic thanks to the presence of no accessible metal sites and to the hydrophobic character of the benzene linker. A plateau is attained at about $P/P_0 = 0.5$, followed by an additional increase from $P/P_0 = 0.8$, possibly correlated with multilayer adsorption. Water adsorption isotherms were performed also on DA-protected and 3P1PA-protected HKUST-1, the most efficient alkyl and aromatic amines, respectively. Compared to the unprotected HKUST-1, the two isotherms showed different shapes. The sigmoidal trend of the as-synthetized MOF is replaced by a logarithmic growth for both protected materials, confirming the enhanced hydrophobicity of the protected materials, in agreement with the impedance spectroscopy measurements. In particular, the functionalization with 3-phenyl-1-propylamine seems to be the most promising one for both the techniques, confirming the utility of combining the two analyses in order to have a more complete result. In fact, the shape of the water isotherm speaks for almost no interaction with water; only 2 mmol g^{-1} at $P/P_0 = 1.0$ are adsorbed. Accordingly, the κ-value for 3P1PA is roughly stable over time (see Figure 8). The slightly worse performance of DA compared to 3P1PA emerges from the reported graphs. For example, the dielectric constant values at low frequency collected after several hours of air exposition show a significant increase of κ especially at low frequency ($\Delta\kappa(1Hz) = +23\%$).

In order to appreciate the effect of pelleting, another water isotherm was collected on a pellet of the DA sample and compared to the powder sample (See figure 9b). As expected, due to the close packing of the particles (hence the smaller accessible surface), water adsorption for a pellet is significantly lower, while featuring a similar shape. In fact, in both cases the trend is logarithmic but at $P/P_0 = 1$ the amount of the adsorbed water is less than 60% for the pellet compared to the powders.

4. Conclusions

The main hypothesis underneath the application of MOFs as low-κ materials is the ideally empty space surrounded by an insulating framework, that they by definition could

guarantee. This feature reduces κ, being it approximately the average between vacuum and the hypothetically dense framework. Thus, the larger is the proportion of empty space, the more efficient should the material be.

Unfortunately, hygroscopicity makes most of highly porous MOFs extremely vulnerable because easily and rapidly filled by water molecules inevitably present in the atmosphere with which the material is in contact. H_2O is the real killer of a low dielectric constant because it is strongly polar, highly polarizable, and easily mobile inside the MOF channels. Thus, water increases both the polarizability of the material electron density and the electric field induced re-orientation and translation of molecular dipoles.

In this work, we have investigated how one very important and often studied MOF, namely HKUST-1 based on the $Cu_3(BTC)_2$ framework, can be protected and significantly increase its hydrophobic behavior to overcome the main limitation for its usage as low-κ materials for advanced microelectronics applications. Among the various remediations reported in the literature, we focused on a recently proposed methodology, the composite of MOF and a surface reacted amine [8]. For this purpose, we tested several aromatic and aliphatic (medium-long chain) amines, to check the overall success of the strategy and address which amine displays the most promising behavior.

The results presented and discussed in the previous sections enable drawing some conclusions:

- HKUST-1 is known to be a highly porous and hydrophilic material, and our experiments demonstrate that it is also stable in electric field. In fact, no significant distortion of the framework is observed upon application of an external voltage. On another perspective, although the water guest molecules in the pores and channels are indeed sensible to the application of a field, they do not order significantly to become more observable than in the absence of a field.
- The diffraction experiments on HKUST-1 after the exchange of the guest from water to CH_2Br_2, reveal the differences between the two topological classes of pores: the tetrahedral (smaller) cavities trap CH_2Br_2, whereas the octahedral (larger) cavities cannot block them. This obviously implies that also smaller guest molecules experience different kind of interactions with the framework depending on the pore in which they enter. So far, only the kind of binding to the framework was distinguishable (at Cu(II) sites, at the carboxylic groups of the linkers, or without any direct interaction with the framework).
- The tested amine surface reaction significantly improves the transformation of HKUST-1 (or in principle other MOFs) into a truly hydrophobic material, while maintaining its crystallinity. The main proofs of this statement are: a) the reduced adsorption of water in the bulk, as proved by gravimetric and adsorption isotherm experiments; b) the small values and the significant stability of the dielectric constant along the range of the scanned frequencies; c) the stability over time of the low dielectric conditions. The last point, however, requires further testing and likely optimization of the fabrication techniques.
- The comparison between vapour adsorption isotherms and dielectric constant measurement indicates that a new perspective can be adopted when investigating the adsorption properties of MOFs. The measurement of dielectric constant is quite rapid (although requiring a significant amount of material) and provides a response agrees with the traditionally adopted adsorption isotherms. In particular, the protected MOFs (except for 1-NTA) reveal a single stage mechanism, which is evident from κ(1Hz) being quite similar to κ(1MHz) and growing linearly with time, instead of exponentially.
- Although in this work we have explored only a limited number of amines, it seems evident that an alkyl chain improves the performance of the amine. Indeed, although 3P1PA (the most efficient) can be classified as an aromatic amine, it possesses a medium length chain separating the aromatic ring from the amino group. On the other hand, amino group directly linked to the aromatic ring do not seem to be so efficient,

especially true for 1NTA (featuring a hindered aromatic system). Probably the combination of aromatic ring and alkyl chain is the best solution, because combining the anchoring ability to framework binding sites, typical of flexible alkylic chains, and the inherent hydrophobicity of aromatic rings.

Further work is needed to identify the most efficient amine (testing a larger group of them). The best amine should be able to guarantee the highest performances and the longer stability of the material over time, which has not been investigated in this work.

A final remark should not escape the reader's attention. In this work we have adopted impedance spectroscopy to semi-quantitatively assess the amount of water adsorbed by a MOF and correlate the observed signals with the kind of guest adsorption into the pores. This technique could become complementary to other well accessed methodologies of measuring the water adsorption and could potentially be used also with other kinds of guests.

Supplementary Materials: The following supporting information can be downloaded at: www.mdpi.com/xxx/s1, powder X-ray diffraction measurements of all the samples tested (Figure S1, as synthesized powders; Figure S2, pellets obtained from compression of the powders); Table of the single crystal X-ray diffraction experiments (Table S1). cif files and checkcif reports for all single crystal X-ray diffraction experiments (**1a**, **1b**, **1c**; **2a**, **2b**, **2c**).

Author Contributions: Conceptualization, P.M. and S.S.; methodology, P.M., S.S., N.C., V.C. and F.B.; software, P.M.; resources, P.M.; data curation, S.S., N.C. and F.B.; writing—original draft preparation, P.M.; writing—review and editing, P.M. and S.S.; funding acquisition, P.M. All authors have read and agreed to the published version of the manuscript.

Funding: This research was funded by Italian MIUR (PhD grant for S.S.), the Polytechnic of Milan (Research Grant for P.M.) and the center for high performance computing CINECA (project POLDIPOL). V.C. thanks the Italian MUR for partial funding through the PRIN2017 project "Moscato n° 2017KKP5ZR) and Università degli Studi di Milano (Transition grant PSR2015-1721VCOLO_01).

Data Availability Statement: In this section, please provide details regarding where data supporting reported results can be found, including links to publicly archived datasets analyzed or generated during the study. Please refer to suggested Data Availability Statements in section "MDPI Research Data Policies" at https://www.mdpi.com/ethics. If the study did not report any data, you might add "Not applicable" here.

Acknowledgments: we thank Mr. Michael Lange for assisting during the experiments at SLS.

Conflicts of Interest: The authors declare no conflict of interest.

References 558

1. Hideshi, M.; Kenji, I.; Makoto, S.; Masaru, H. Review of methods for the mitigation of plasma-induced damage to low-dielectric-constant interlayer dielectrics used for semiconductor logic device interconnects. *Plasma Process Polym.* **2019**, 16, e1900039. DOI: 10.1002/ppap.201900039.
2. Usman, M.; Lu, K.L. Metal-organic frameworks: the future of low-κ materials. NPG Asia Materials. 2016, 8, e333. DOI: 10.1038/am.2016.175
3. Eddaoudi, M.; Moler, D.B., Li, H.; Chen, B.; Reineke, T.M.; O'Keeffe, M.; Yaghi, O.M. Modular chemistry: secondary building units as a basis for the design of highly porous and robust Metal-Organic Carboxylate Frameworks. *Acc. Chem Res.* **2001**, *34*, 319-330. DOI: 10.1021/ar000034b.
4. Chen, Z.; Kirlikovali, O.K.; Li, P.; Farha, O.K. Reticular chemistry for highly porous Metal-Organic Frameworks: the chemistry and applications. *Acc. Chem Res.* **2022**, *55*, 579-591. DOI: 10.1021/acs.accounts.1c00707.
5. Howarth, A. J.; Liu, Y.; Li, P.; Li, Z.; Wang, T. C.; Hupp, J. T.; Farha, O. K. Chemical, thermal and mechanical stabilities of metal–organic frameworks. *Nat. Rev. Mater*. **2016**, *1*, 15018. doi: 10.1038/natrevmats.2015.18
6. Kim, H.; Rao, S. R.; Kapustin, E. A.; Zhao, L.; Yang, S.; Yaghi, O. M., Wang, E. N. Adsorption-based atmospheric water harvesting device for arid climates. *Nature Comm*. **2018**, *9*, 1191. DOI: 10.1038/s41467-018-03162-7.
7. Zhang, W.; Hu, Y.; Ge, J.; Jiang H.L.; Yu, S.H. A Facile and General Coating Approach to Moisture/Water-Resistant Metal–Organic Frameworks with Intact Porosity. *J. Am. Chem. Soc.* **2014**, *136*, 16978-16981. DOI: 10.1021/ja509960n.
8. Gao, M.L.; Zhao, S.Y.; Chen, Z.Y.; Liu, L.; Han, Z.B. Superhydrophobic/Superoleophilic MOF Composites for Oil–Water Separation. *Inorg. Chem*. **2019**, *58*, 2261-2264. DOI: 10.1021/acs.inorgchem.8b03293.
9. Chui, S. S.-Y.; Lo, S. M.-F.; Charmant, J. P. H.; Orpen, A. G.; Williams, I. D. Chemically Functionalizable Nanoporous Material $[Cu_3(TMA)_2(H_2O)_3]_n$ *Science*, **1999**, *283*, 1148-1150. DOI: 10.1126/science.283.5405.1148.
10. Ghoufi, A.; Benhamed, K.; Boukli-Hacene, L.; Maurin, G. Electrically Induced Breathing of the MIL-53(Cr) Metal–Organic Framework, *ACS Cent. Sci.* **2017**, *3*, 394-398. DOI: 10.1021/acscentsci.6b00392.
11. Wu, Y.; Kobayashi, A.; Halder, G. J.; Peterson, V. K.; Chapman, K. W.; Lock, N.; Southon, P. D.; Kepert, C. J., Negative thermal expansion in the metal-organic framework material Cu_3(1,3,5-benzenetricarboxylate)$_2$. *Angew. Chem.*, Int. Ed. **2008**, *47*, 8929–8932. DOI: 10.1002/anie.200803925.
12. Schlichte, K.; Kratzke, T.; Kaskel, S. Improved synthesis, Thermal Stability and Catalytic Properties of The Metal-Organic Framework Compound $Cu_3(BTC)_2$. *Microporous Mesoporous Mater*. **2004**, 73, 81–88. DOI: 10.1016/j.micromeso.2003.12.027.
13. Willmott, P. R; Meister, D; Leake, S. J; Lange, M; Bergamaschi, A; Boge, M; Calvi, M; Cancellieri, C; Casati, N; Cervellino, A; Chen, Q; David, C; Flechsig, U; Gozzo, F; Henrich, B; Jaggi-Spielmann, S; Jakob, B; Kalichava, I; Karvinen, P; Krempasky, J; Ludeke, A; Luscher, R; Maag, S; Quitmann, C; Reinle-Schmitt, M. L; Schmidt, T; Schmitt, B; Streun, A; Vartiainen, I; Vitins, M; Wang, X; Wullschleger, R. The Materials Science beamline upgrade at the Swiss Light Source. *J. Synchrotron Rad.* **2013**, *20*, 667-682. DOI: 10.1107/S0909049513018475.
14. Rigaku Oxford Diffraction, (2021), CrysAlisPro Software system, version 171.41.93a, Rigaku Corporation, Oxford, UK
15. Dolomanov, O.V.; Bourhis, L.J.; Gildea, R.J.; Howard, J.A.K.; Puschmann, H. OLEX2: a complete structure solution, refinement and analysis program. *J. Appl. Cryst.* **2009**, *42*, 229–341 DOI: 10.1107/S0021889808042726.
16. Macrae, C. F.; Sovago, I.; Cottrell, S. J.; Galek, P. T. A.; McCabe, P.; Pidcock, E.; Platings, M.; Shields, G. P.; Stevens, J. S.; Towler, M.; Wood, P. A. Mercury 4.0: from visualization to analysis, design and prediction. *J. Appl. Cryst.*, **2020**, *53*, 226-235. DOI: 10.1107/S1600576719014092.
17. Becke, A. D. J. Density-functional thermochemistry. III. The role of exact exchange. *Chem. Phys*. **1993**, *98*, 5648-5652. DOI: 10.1063/1.464913.
18. Lee, C.; Yang, W.; Parr, R. G. Development of the Colle-Salvetti correlation-energy formula into a functional of the electron density. *Phys. Rev. B* **1988**, 37, 785-789. DOI: 10.1103/PhysRevB.37.785.
19. Weigend, F.; Ahlrichs, R. Balanced Basis Sets of Split Valence, Triple Zeta Valence and Quadruple Zeta Valence Quality for H to Rn: Design and Assessment of Accuracy. *Phys. Chem. Chem. Phys*., **2005**, 7, 3297-3305. DOI: 10.1039/B508541A.
20. Weigend, F. Accurate Coulomb-fitting basis sets for H to Rn. *Phys. Chem. Chem. Phys*., **2006**, *8*, 1057-1065. DOI: 10.1039/B515623H.
21. Gaussian 16, Revision C.01, Frisch, M. J.; Trucks, G. W.; Schlegel, H. B.; Scuseria, G. E.; Robb, M. A.; Cheeseman, J. R.; Scalmani, G.; Barone, V.; Petersson, G. A.; Nakatsuji, H.; Li, X.; Caricato, M.; Marenich, A. V.; Bloino, J.; Janesko, B. G.; Gomperts, R.; Mennucci, B.; Hratchian, H. P.; Ortiz, J. V.; Izmaylov, A. F.; Sonnenberg, J. L.; Williams-Young, D.; Ding, F.; Lipparini, F.; Egidi, F.; Goings, J.; Peng, B.; Petrone, A.; Henderson, T.; Ranasinghe, D.; Zakrzewski, V. G.; Gao, J.; Rega, N.; Zheng, G.; Liang, W.; Hada, M.; Ehara, M.; Toyota, K.; Fukuda, R.; Hasegawa, J.; Ishida, M.; Nakajima, T.; Honda, Y.; Kitao, O.; Nakai, H.; Vreven, T.; Throssell, K.; Montgomery, J. A., Jr.; Peralta, J. E.; Ogliaro, F.; Bearpark, M. J.; Heyd, J. J.; Brothers, E. N.; Kudin, K. N.; Staroverov, V. N.; Keith, T. A.; Kobayashi, R.; Normand, J.; Raghavachari, K.; Rendell, A. P.; Burant, J. C.; Iyengar, S. S.; Tomasi,

J.; Cossi, M.; Millam, J. M.; Klene, M.; Adamo, C.; Cammi, R.; Ochterski, J. W.; Martin, R. L.; Morokuma, K.; Farkas, O.; Foresman, J. B.; Fox, D. J. Gaussian, Inc., Wallingford CT, 2016.

22. Krawczuk, A.; Pérez, D.; Macchi, P. J. PolaBer: A Program to Calculate and Visualize Distributed Atomic Polarizabilities Based on Electron Density Partitioning. *Appl. Cryst.* **2014**, *47*, 1452–1458. DOI: 10.1107/S1600576714010838.
23. Bader R. F. W. *Atoms in Molecules: A Quantum Theory* Oxford University Press: New York, U. S., 1990.
24. Keith, T. A. AIMAll. Version 19.10.12. TK Gristmill Software, Overland Park KS, 2019.
25. Bader, R.; Keith, T.; Gough, K.; Laidig, K. Properties of Atoms in Molecules: Additivity and Transferability of Group Polarizabilities. *Mol. Phys.* **1992**, *75*, 1167–1189. DOI: 10.1080/00268979200100901.
26. Nye, J. F. *Physical Properties of Crystals: Their Representation by Tensors and Matrices*. Oxford University Press: Oxford, U.K., 1957.
27. Scatena, R.; Guntern, Y. T.; Macchi, P. Electron Density and Dielectric Properties of Highly Porous MOFs: Binding and Mobility of Guest Molecules in $Cu_3(BTC)_2$ and $Zn_3(BTC)_2$. *J. Am. Chem. Soc.*, **2019**, *141*, 9382–9390. DOI: 10.1021/jacs.9b03643.
28. Kitagawa, S.; Kitaura, R.; Noro, S.-I. Functional Porous Coordination Polymers. *Angew. Chem. Int. Ed*. **2004**, *43*, 2334–2375. DOI: 10.1002/anie.200300610.
29. Talin, A.A.; Centrone, A.; Ford, A.C.; Foster, M.E.; Stavila, V.; Haney, P.; Kinney, R.A.; Szalai, V.; Gabaly, F.El.; Yoon, H.P.; Léonard F.; Allendorf, M.D. Tunable electrical conductivity in metal-organic framework thin-film devices. *Science*. **2014**, *343*, 66-69. DOI: 10.1126/science.1246738.
30. Canivet, J.; Fateeva, A.; Guo, Y.; Coasne, B.; Farrusseng, D. Water adsorption in MOFs: fundamentals and applications. *Chem. Soc. Rev.* **2014**, *43*, 5594-5617. DOI: 10.1039/C4CS00078A.
31. Álvarez, J.R.; Sánchez-González, E.; Pérez, E.; Schneider-Revueltas, E.; Martínez, A.; Tejeda-Cruz, A.; Islas-Jácome, A.; González-Zamora, E.; Ibarra, I. A. Structure stability of HKUST-1 towards water and ethanol and their effect on its CO_2 capture properties. *Dalton Trans.* **2017**, *46*, 9192-9200. DOI: 10.1039/C7DT01845B.
32. Küsgens, P.; Rose, M.; Senkovska, I.; Fröde, H.; Henschel, A.; Siegle, S.; Kaskel, S. Characterization of metal-organic frameworks by water adsorption. *Microporous Mesoporous Mater.* **2009**, *120*, 325-330. DOI: 10.1016/j.micromeso.2008.11.020.
33. Janiak, C.; Henninger, S.K. Porous coordination polymers as novel sorption materials for heat transformation processes. *Chimia*. **2013**, *67*, 419-424. DOI: 10.2533/chimia.2013.419.